Assessment of the GPM and TRMM Precipitation Products Using the Rain Gauge Network over the Tibetan Plateau

Sijia ZHANG[1,2], Donghai WANG[2], Zhengkun QIN[1*], Yaoyao ZHENG[3], and Jianping GUO[4]

1 *Joint Center for Data Assimilation Research and Applications*, *Nanjing University of Information Science &Technology*, *Nanjing* 210044, *China*
2 *School of Atmospheric Sciences*, *Sun Yat-Sen University*, *Zhuhai* 519082, *China*
3 *Institute of Meteorology and Climate Research*, *Karlsruhe Institute of Technology*, *Karlsruhe* 76021, *Germany*
4 *State Key Laboratory of Severe Weather*, *Chinese Academy of Meteorological Sciences*, *Beijing* 100081, *China*

(Received May 19, 2017; in final form November 3, 2017)

ABSTRACT

Using high-quality hourly observations from national-level ground-based stations, the satellite-based rainfall products from both the Global Precipitation Measurement (GPM) Integrated MultisatellitE Retrievals for GPM (IMERG) and its predecessor, the Tropical Rainfall Measuring Mission (TRMM) Multi-satellite Precipitation Analysis (TMPA), are statistically evaluated over the Tibetan Plateau (TP), with an emphasis on the diurnal variation. The results indicate that: (1) the half-hourly IMERG rainfall product can explicitly describe the diurnal variation over the TP, but with discrepancies in the timing of the greatest precipitation intensity and an overestimation of the maximum rainfall intensity over the whole TP. In addition, the performance of IMERG on the hourly timescale, in terms of the correlation coefficient and relative bias, is different for regions with sea level height below or above 3500 m; (2) the IMERG products, having higher correlation and lower root-mean-square error, perform better than the TMPA products on the daily and monthly timescales; and (3) the detection ability of IMERG is superior to that of TMPA, as corroborated by a higher Hanssen and Kuipers score, a higher probability of detection, a lower false alarm ratio, and a lower bias. Compared to TMPA, the IMERG products ameliorate the overestimation across the TP. In conclusion, GPM IMERG is superior to TRMM TMPA over the TP on multiple timescales.

Key words: Global Precipitation Measurement, Tropical Rainfall Measuring Mission, Tibetan Plateau, precipitation

Citation: Zhang, S. J., D. H. Wang, Z. K. Qin, et al., 2018: Assessment of the GPM and TRMM precipitation products using the rain gauge network over the Tibetan Plateau. *J. Meteor. Res.*, **32**(2), 324–336, doi: 10.1007/s13351-018-7067-0.

1. Introduction

Precipitation plays a key role in the modulation of the global hydrological cycle and energy balance of the earth (Kidd et al., 2012). Accurate measurements of precipitation over a variety of spatial and temporal scales are important to weather forecasters and climate scientists (Ebert et al., 2007). However, over regions with complex terrain, precipitation measurements from rain gauges and ground-based weather radar usually suffer from the limited spatial coverage (Yong et al., 2012; Guo et al., 2016; Tang et al., 2016). The Tibetan Plateau (TP) is an example of a region with complex terrain and insufficient ground-based measurements. Satellites can usually provide observations of precipitation at broader geographical scales (Kidd and Levizzani, 2011; Kidd et al., 2012; Hou et al., 2014), and thus, satellite-derived rainfall estimations offer considerable potential in obtaining higher-quality precipitation measurements over the TP.

Since the launch of the Tropical Rainfall Measuring Mission (TRMM) (Simpson et al., 1988; Hong et al., 2004) in 1997, satellite-derived precipitation products have gradually achieved a good level of maturity (Kidd and Levizzani, 2011). Currently, there are a variety of

Supported by the National Natural Science Foundation of China (91437221 and 41775097), Science and Technology Planning Project of Guangdong Province (2017B020218003), and Natural Science Foundation of Guangdong Province (2016A030313140).

*Corresponding author: qzk_0@nuist.edu.cn.

satellite-derived rainfall products available, including the TRMM Multi-satellite Precipitation Analysis (TMPA) (Huffman et al., 2007), the Climate Prediction Center morphing technique (CMORPH) (Joyce et al., 2004), and the Precipitation Estimation from Remotely Sensed Information using Artificial Neural Networks (PERSIANN) (Hsu et al., 1997; Sorooshian et al., 2000; Hong et al., 2004). Previous studies have found that the TMPA precipitation products outperform other satellite products (e.g., PERSIANN and CMORPH) across the TP in terms of lower errors and biases (Gao and Liu, 2013; Tong et al., 2014).

As TRMM's successor, the Global Precipitation Measurement (GPM) mission aims to set a new standard for spaceborne quantitative precipitation estimation and provide the next generation of precipitation products. Launched on 28 February 2014, the GPM Core Observatory, carrying the first spaceborne dual-frequency precipitation radar (DPR) and a conical-scanning multi-channel microwave imager, was designed with a wider measurement range compared with TRMM (Hou et al., 2014). The GPM mission provides Level-3 Integrated MultisatellitE Retrievals for GPM (IMERG) Final Run products at half-hourly and monthly temporal resolutions and at a spatial resolution of 0.1°.

Research has been carried out to evaluate IMERG on the monthly, daily, and hourly temporal scales. The IMERG monthly product is able to capture the major heavy precipitation regions reasonably well (Liu, 2016), and outperforms its predecessor (TMPA) on the seasonal and monthly timescales over mainland China (Chen and Li, 2016; Guo et al., 2016). Besides, the IMERG half-hourly product has also been evaluated on the daily and sub-daily timescales (Oliveira et al., 2016; Prakash et al., 2016; Tang et al., 2016; Wen et al., 2016). For instance, the diurnal variation over the Brazilian Amazon rainforest has been shown to be well represented by IMERG (Oliveira et al., 2016). Moreover, on the three-hourly timescale, IMERG has been shown to perform better than TRMM 3B42V7, based on a slightly higher level of correlation and lower bias (Ma et al., 2016). However, most of the aforementioned studies only analyzed IMERG data over a period of less than 1 yr. Moreover, to the best of our knowledge, few studies have evaluated the IMERG products on the hourly scale against hourly rainfall intensity observations, or evaluated its capability in representing the diurnal variation over mountainous regions.

The TP is the largest and highest plateau in the world, and its topographic characteristics exert significant influences upon the weather and climate over Eurasia. A high-quality gauge network over the TP, established with national-level terrestrial gauge stations (Shen et al., 2010), is used in the present study alongside the satellite datasets introduced above to: (1) evaluate the quality of the GPM IMERG half-hourly precipitation product (hereafter referred to as IMERG_HHR) over the TP, and (2) compare the IMERG_HHR and monthly precipitation (hereafter referred to as IMERG_MO) products with their predecessors, the TMPA 3-h 3B42V7 (hereafter referred to as TMPA_3HR) and monthly 3B43 (hereafter referred to as TMPA_MO) products. We begin by focusing on the diurnal variation of precipitation over the TP before moving on to analyzing both the daily and monthly timescales to reveal the continuity and differences between the IMERG and TMPA products. In doing so, we hope to provide a useful reference for research and applications over complex terrain during the transition from TMPA to IMERG.

Following this introduction, the study area, datasets, and evaluation methods are described in Section 2. Section 3 evaluates the GPM IMERG satellite data through comparison with the ground-based rain gauge data, with a focus on analyzing the diurnal variability of the rainfall illustrated by the IMERG_HHR product in the summer season. Besides, this section also compares the IMERG products with the TMPA products on the daily and monthly timescales over the TP. Section 4 summarizes the key findings of our study.

2. Study area, datasets, and methodology

The study area spans over 26°00′–39°47′N, 73°19′–104°47′E. This part of the TP typically experiences frequent precipitation events and is characterized by strong diurnal variation in precipitation during summer under certain large-scale atmospheric conditions (Liu et al., 2002; Bai et al., 2008; Singh and Nakamura, 2009; Guo et al., 2014).

Ground-based rain gauge measurements provided by the National Meteorology Information Center (NMIC) of the China Meteorological Administration (CMA) are used as the reference datasets in this study. Hourly precipitation measurements from a national network of approximately 2000 national-level automatic weather stations are processed with strict quality control (Shen et al., 2010), and have been used as surface reference datasets in several other local and regional rainfall studies (Shen et al., 2010, 2014; Ma et al., 2016). Figure 1 shows the spatial distribution of the national-level ground-based observation stations. Both the IMERG and TMPA products use the precipitation information of the Global Precipitation Climatology Center (GPCC) gauge dataset for bias

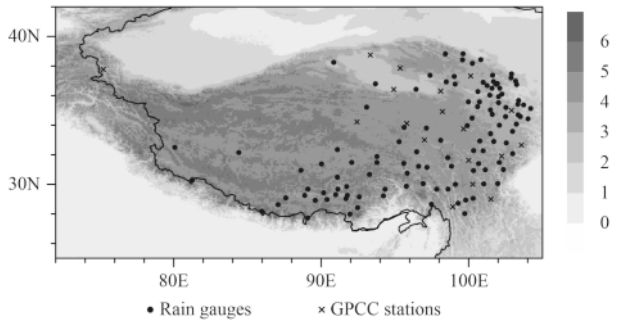

Fig. 1. Spatial distribution of national-level ground-based observation stations over the TP, in which dots represent the independent stations used in the present study and crosses denote the stations applied in the GPCC dataset. The uneven shading indicates the elevation (km).

adjustment. Our study excludes the data from the stations that are part of the GPCC (denoted by crosses in Fig. 1), which is different from the approach in previous work (Guo et al., 2016; Ma et al., 2016). Such a strategy, being solely based on 113 stations that are independent from the GPCC dataset (denoted by dots in Fig. 1) could be more scientifically rigorous. The topographic information in Fig. 1 is provided by the global elevation and bathymetry from the 2 arc-minute grid (ETOPO2) dataset.

The TMPA provides a calibration-based sequential scheme for combining precipitation estimates from multiple satellites, as well as rain-gauge analyses from the GPCC Monitoring Product Version 4. The temporal resolutions of the TMPA products are three-hourly and monthly, with a spatial resolution of 0.25° × 0.25° and spatial coverage over 50°N–50°S. The TRMM data officially stopped on 8 April 2015 with the decommission of the TRMM Microwave Imager (TMI), marking the transition from the TRMM products to the GPM mission products. Thus, intercalibration of the passive microwave (PMW) precipitation estimates from TRMM after 8 April 2015 may to some extent suffer from inhomogeneity with previous data. Based on this consideration, the latest 3-h 3B42 Version 7 product and monthly 3B43 product from April 2014 to December 2015 are used in this study. These products are research-level products, appropriate for scientific purposes.

IMERG is designed to inter-calibrate, merge, and interpolate all possible satellite microwave precipitation estimates, accompanied by microwave-calibrated infrared satellite estimates, gauge precipitation analyses, and other potential precipitation estimators. IMERG employs the 2014 version of the Goddard Profiling Algorithm (GPROF2014), which improves the precipitation estimation computation from all passive microwave sensors, compared with TMPA (GPROF2010). Similar to TMPA, IMERG also provides near-real-time products—the IMERG Early Run and Late Run—as well as the post-real-time IMERG Final Run product. Nevertheless, the products of IMERG feature a finer spatial (0.1° × 0.1°) and higher temporal (half-hourly) resolution compared with TMPA products. In our study, we use both the half-hourly and monthly IMERG Final Run Version 3 products, which again are research-level products.

Point-to-pixel evaluation is performed between the rain gauge and gridded satellite data. Station-based rain gauge data are utilized rather than gridded rain gauge data for two reasons. First, performing interpolation from station-based measurements to a gridded dataset would unavoidably introduce further systematic errors. Second, the distribution of precipitation over the TP is characterized by high spatial heterogeneity, and thus, interpolation might smooth out the small-scale variations of precipitation related to the interaction between the highly varied topography and the atmospheric flow. Regardless of the different spatial resolutions of the IMERG and TMPA products (0.1° and 0.25°), the nearest-neighbor interpolation method is applied. The closet pixel from each satellite overpass for each rain gauge is located. The precipitation rate from rain gauges closest to the scanning time of that satellite overpass is extracted. Thus, the precipitation rate from a satellite pixel can be matched with the coincident precipitation rate from rain gauges to generate pairings of satellite-gauge data for evaluation and comparison.

The study period is from April 2014 to December 2015; however, for the diurnal variation, we only focus on the summer season (June–September). Owing to the limited sensitivity of the tipping-bucket rain gauge instrument, rainfall rates of less than 0.1 mm are set to zero. Therefore, a "precipitation hour" refers to a 1-h period when the accumulated rainfall rate is no less than 0.1 mm. In addition, a naming scheme for time division proposed by Singh and Nakamura (2009) is used. In this scheme, each daily 24-h period is divided into eight 3-h intervals based on local standard time (LST): late night (0000–0300 LST); early morning (0300–0600 LST); morning (0600–0900 LST); late morning (0900–1200 LST); early afternoon (1200–1500 LST); late afternoon (1500–1800 LST); evening (1800–2100 LST); and night (2100–2400 LST).

Next, we describe the methodology used to evaluate the performance of the satellite rainfall products. Two kinds of probability density functions (PDFs) are used: one is computed as the ratio between the number of rain rates under different rainfall intensities to the total number of rain rates, which is called "PDFs by occurrence"

(PDFc); and the other represents the relative volumetric contribution of the rain rates under different rainfall intensities to the total rainfall volume, which is called "PDFs by rain volume" (PDFv) (Kirstetter et al., 2013). Those metrics have been widely used to describe rainfall distributions from the perspectives of frequency and volume, respectively (Wolff and Fisher, 2009; Shen et al., 2010; Kirstetter et al., 2013; Prat and Nelson, 2013; Guo et al., 2016; Xu et al., 2017). The Taylor diagram (Taylor, 2001) is used to determine the impact of elevation on the accuracy of the satellite precipitation products. On the Taylor diagram, the radial coordinate is the magnitude of the normalized standard deviation, while the angular coordinate denotes the correlation coefficient (CC). The relative bias is given by the shape and size of the markers. The closer the marker gets to the observation—the intersection point of the concentric black dotted lines and the axis—the better the test field performs.

In addition to the PDF and Taylor diagram, the performance of the satellite-based precipitation estimates is also evaluated by using continuous and categorical statistical metrics. The continuous statistical metrics include the CC, root-mean-square error (RMSE), and relative bias. The categorical statistical metrics include the probability of detection (POD), which presents the fraction of precipitation events that are correctly detected by estimates; the false alarm ratio (FAR), which shows the fraction of events that are misinterpreted as events; the bias score (BIAS), which gives the ratio of the estimated and observed rain pixels; and the Hanssen and Kuipers score (HKS). The formulas and perfect values for these metrics are given in Table 1, with more details available in Sapiano and Arkin (2009) and Cimini et al. (2013).

Table 1. List of continuous and categorical statistical metrics used for evaluation

Statistical metric	Formula	Perfect value
CC	$\frac{1}{N}\sum_{i=1}^{N}\left(S_i-\bar{S}\right)\left(G_i-\bar{G}\right)/(\sigma_S\sigma_G)$	1
RMSE	$\sqrt{\frac{1}{N}\sum_{i=1}^{N}(S_i-G_i)^2}$	0
Relative Bias	$\sum_{i=1}^{N}(S_i-G_i)/\sum_{i=1}^{N}G_i$	0
POD	$H/(H+M)$	1
FAR	$F/(H+F)$	0
BIAS	$(H+F)/(H+M)$	1
HKS	$H/(H+M)-F/(F+T)$	1

Notation: N, number of samples; G_i, rain-gauge observed precipitation; S_i, satellite precipitation estimates; σ_G and σ_S, standard deviation of rain-gauge and satellite precipitation, respectively. Every satellite-gauge match-up can be classified as a hit (H, observed rain correctly detected), a miss (M, observed rain not detected), a false alarm (F, rain detected but not observed), or a correct null (T, no rain observed nor detected) event.

3. Results and discussion

3.1 *Evaluation on the hourly timescale*

In this section, we evaluate IMERG_HHR on the hourly timescale. We start the evaluation with two PDFs, and then focus on the capability of IMERG_HHR to characterize the diurnal variation of rainfall through consideration of several aspects, including the overall tendency, the spatial distribution of the rainfall peak, and the impact of elevation. The summer seasonal diurnal cycle is described by using the mean hourly rainfall intensities of 244 days, and converted from UTC to LST for each gauge station.

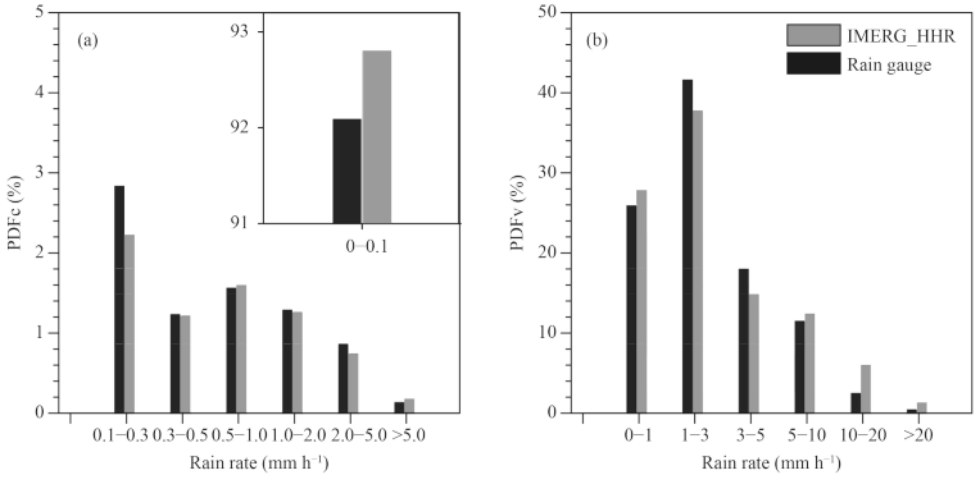

Fig. 2. (a) Probability density function by occurrence (PDFc) and (b) probability density function by volume (PDFv) of hourly precipitation with different intensities from IMERG_HHR and rain gauges over the TP.

Figure 2 shows the PDFc and PDFv of hourly precipitation over the TP. As shown in the top-right corner of Fig. 2a, most of the hourly rainfall intensity falls in the 0–0.1 mm h^{-1} bin, which is denoted as "no rain", and IMERG_HHR matches this well with a negligible overestimation (0.71%). IMERG_HHR tends to miss 0.61% of rainfall events of which the hourly rainfall intensity is within 0.1–0.3 mm h^{-1} (Fig. 2a). It also underestimates the PDFv of less than 1 mm h^{-1} for 3.9%, and the primary underestimation comes from missing detections within 0.1–0.3 mm h^{-1}, as shown in Fig. 2a. Furthermore, the underestimation of the PDFv for 1–10 mm h^{-1} may be caused by the underestimation of the PDFc, due to the insufficient detection capability. The overestimation of IMERG in the total rainfall volume of intense rainfall categories (hourly intensity larger than 10 mm h^{-1}) in Fig. 2b may be attributable to the overestimation in both the frequency of occurrence and the values of rainfall intensity. These discrepancies may be due to several factors: First, the PMW-based algorithms of IMERG still tend to miss shallow and warm precipitation (Andermann et al., 2012; Shige et al., 2013). In addition, the complicated terrain, evaporation processes, and inconsistency between gauge-station and satellite datasets (caused by the sparse coverage of the former) may also lead to discrepancies (Guo et al., 2016).

Next, on the basis of the above evidence that IMERG_HHR is reliable at capturing rainfall events on the hourly scale, the capability of IMERG_HHR in characterizing the diurnal variation of precipitation is discussed. The results for the summer seasons in 2014 and 2015 are plotted in Fig. 3. As we can see, both the gauge measurements and IMERG_HHR reveal a strong peak in mean precipitation intensity in the evening and a minimum in the late morning, disclosing an obvious diurnal cycle over the TP. The variations demonstrated by IMERG_HHR and the rain-gauge data are similar, and thus, we can infer that the IMERG_HHR products can explicitly describe the diurnal variation over the TP. Analyses of the diurnal cycle spanning from March to September (not shown) also demonstrate similarity between the rain-gauge measurements and the IMERG_HHR data.

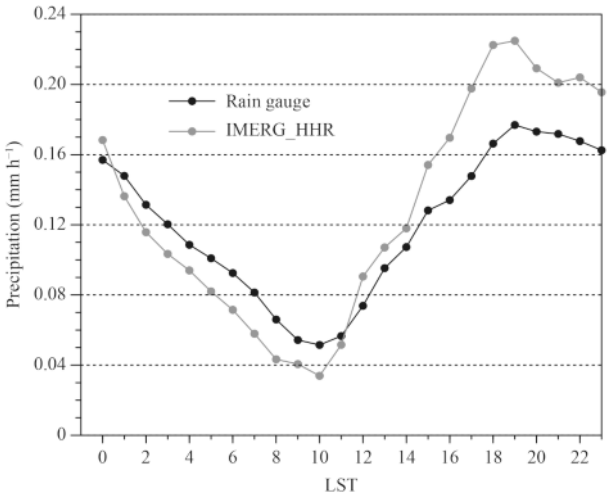

Fig. 3. Diurnal cycle of precipitation over the TP in the summer seasons of 2014 and 2015. Results are derived from the half-hourly precipitation estimates of GPM IMERG_HHR and the hourly rain-gauge data used as a reference, and converted to local standard time (LST).

Table 2 shows the proportion and average intensity from the rain-gauge data and from IMERG_HHR during the 3-h periods in which the maximum hourly rainfall occurs. Eighty stations among the total 113 (70.8%) experience their greatest precipitation intensity form late afternoon to late night. IMERG_HHR underestimates the occurrence frequency of the afternoon-to-evening peak by 34.52%. The average rainfall estimates of IMERG_HHR are quite close to that of the gauge measurements during 0600–0900 and 1200–1800 LST, while IMERG_HHR overestimates the intensity of the late-morning peak by 0.16 mm h^{-1}. Regarding nocturnal precipitation, IMERG_HHR presents an obvious mismatch in the maximum hourly rainfall phase and an overestimation in the maximum hourly rainfall intensity—in particular, the occurrence frequency of the nighttime peak and the maximum rainfall intensity during 0000–0600 LST.

Table 2. Occurrence frequency and average intensity of precipitation from rain-gauge measurements and IMERG_HHR during the 3-h periods in which the maximum hourly rainfall intensity occurs. Maximum intensity is calculated by using data whose frequency of occurrence is above 95%, thus avoiding anomalous cases

Time	Period (LST)	Rain gauge		IMERG_HHR	
		Frequency (%)	Intensity (mm h^{-1})	Frequency (%)	Intensity (mm h^{-1})
Late night	0000–0300	12.39	0.78	15.93	0.97
Early morning	0300–0600	8.85	0.77	14.16	0.95
Morning	0600–0900	3.54	0.86	6.19	0.93
Late morning	0900–1200	7.96	0.88	6.19	1.04
Early afternoon	1200–1500	8.85	0.81	1.77	0.89
Late afternoon	1500–1800	14.16	0.82	4.42	0.86
Evening	1800–2100	28.32	0.81	10.62	0.97
Night	2100–2400	15.93	0.82	40.71	0.95

In order to discern the spatial features of the diurnal peak phase, a vector plot is used. Vector plots can represent the time when the maximum precipitation occurs by the direction of an arrow pointer on a circular 24-h clock dial to clockwise, and the corresponding precipitation intensity (Dai et al., 1999; Guo et al., 2014). Thus, information on both the diurnal phase and amplitude for rainfall measurements can be identified. Figure 4 presents separate vector plots for the rain-gauge measurements and IMERG_HHR over the TP during the summer seasons of 2014 and 2015. Here, the maximum precipitation is calculated by using data whose frequency of occurrence is below 95%, thus avoiding anomalous cases. Past literature in this area shows that the diurnal variation of precipitation is strongly affected by the TP's topography over the complex mountain–valley terrain of its southern region (Fujinami et al., 2005). There are discrepancies in the timing of the precipitation peak between IMERG_HHR and the amplitude of IMERG_HHR over the whole of the TP, as shown in Fig. 4. From the rain-gauge data, a late-afternoon-to-night peak is dominant in the eastern TP region and a morning peak can be observed along the eastern border, whereas IMERG_HHR presents the morning peak more frequently. A general evening-to-night peak of precipitation is observed in the rain-gauge data along the Yarlung-Zangbo River, whereas a peak in the period from late night to early morning dominates according to IMERG_HHR. These discrepancies in the timing of the greatest precipitation intensity between IMERG_HHR and the rain-gauge data are consistent with the analysis of the results presented in Table 2. In addition, the maximum rainfall intensity is overestimated by IMERG_HHR over the whole of the TP, and the overestimation is more obvious when evaluating against gauges whose rainfall diurnal peaks occur during late night to early morning. Nevertheless, in terms of the maximum rainfall intensity amplitude and phase, according to the discussion above, the performance of IMERG_HHR might still need further improvement.

Figure 5 is a Taylor diagram of IMERG_HHR and the rain-gauge data under different elevations. IMERG_HHR shows different performances with the elevation threshold of 3500 m for rain gauges, and the statistics for an elevation lower than 3500 m are better than those for above 3500 m. Downward triangles show an underestimation below 3500 m, and upward triangles show an overestimation at higher than 3500 m. The red upward triangles represent normalized pattern statistics at all the elevations with a CC of 0.39, a ratio of standard deviation of 1.02, and a relative bias of 1.56%. The performances at elevations lower than 3500 m (marked in dark-blue and green) are obviously better than those at elevations higher than 3500 m (marked in brown, light-blue, and yellow), with a larger CC and a smaller relative bias. Xu et al. (2017) also found a similar underestimation at lower elevation and an overestimation at higher elevation, when using a threshold of 3000 m over southern TP, but the relationship between the CC and elevation was not statistically significant. Note, however, that Xu's study on elevation was based on daily data from 63 local domains, whereas our analysis uses hourly data from 113 national-level rain gauges. The different performances of IMERG_HHR on the hourly scale in terms of the CC, relative bias and ratio of standard deviation, with a threshold of 3500 m, suggest that the impact of elevation on the accuracy of satellite precipitation products needs to be further investigated in future studies.

3.2 *Evaluations on the daily and monthly timescales*

Next, based on their correspondence with ground

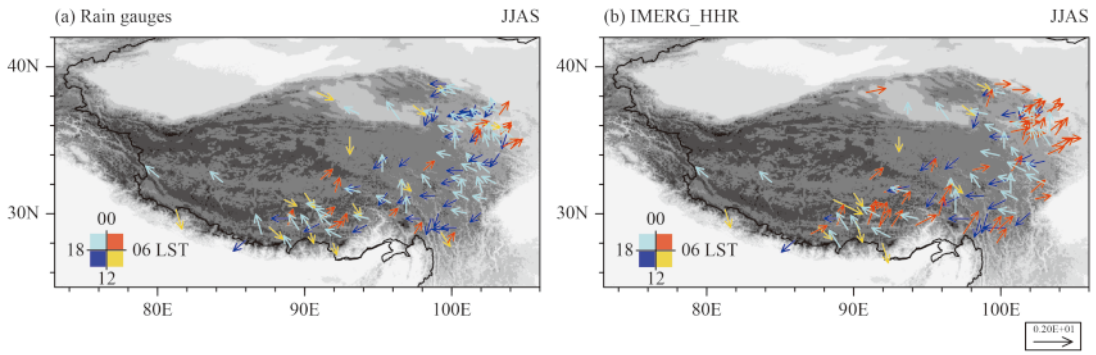

Fig. 4. Spatial distribution of the maximum hourly rainfall intensity and its phase based on (a) gauge measurements and (b) IMERG_HHR, at gauge stations over the TP during the summer seasons of 2014 and 2015. The length of the arrows represents the maximum hourly gauge rainfall intensity. The direction and color of the arrows denote the LST of the maximum at a given gauge station, wherein an orange arrow denotes 0000–0600 LST, yellow denotes 0600–1200 LST, dark blue denotes 1200–1800 LST, and light blue denotes 1800–2400 LST. The reference arrow shown in the bottom-right corner represents 2 mm h^{-1}.

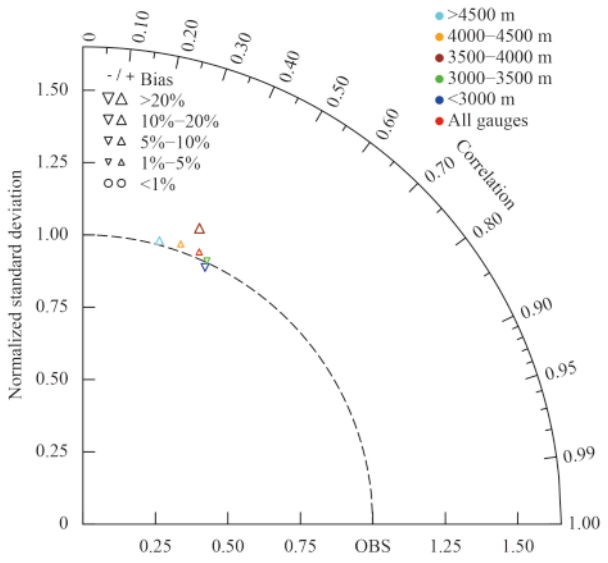

Fig. 5. Taylor diagram showing the correlation coefficient, normalized standard deviation and relative bias between IMERG_HHR and rain-gauge data under different elevations. The azimuthal position denotes the CC. The radial distance from the origin is proportional to the ratio of the normalized standard deviation. The relative bias is given by the shape and size of the markers, as illustrated in the top-left legend. The colors of the markers denote different elevations, as illustrated in the top-right legend.

measurements, we compare the IMERG and TMPA products on the daily and monthly timescales, as well as the effect that elevation has on their respective performances.

Figure 6 intercompares the PDFc and PDFv of the daily and monthly mean rainfall from the gauge measurements and two satellite rainfall products. The performances of IMERG are generally better than the corresponding TMPA products in terms of PDFc and PDFv. On the daily scale, IMERG_HHR demonstrates better ability in capturing light precipitation events (less than 1 mm day^{-1}) than TMPA_3HR (Fig. 6a), and similar improvement of IMERG_HHR over TMPA_3HR in the rainfall volume of light rainfall categories can be seen in Fig. 6b. The better capability of IMERG_HHR in detecting no-rain and light-rain events may be attributable to the DPR carried by the GPM Core Observatory, with its greater sensitivity at light rain rates than the PR onboard the TRMM satellite (Hou et al., 2014). Both IMERG_HHR and TMPA_3HR tend to underestimate the frequency of moderate and heavy rainfall events (larger than 5 mm day^{-1}), as illustrated in Fig. 6a, and underestimate the rainfall volume of moderate rainfall events

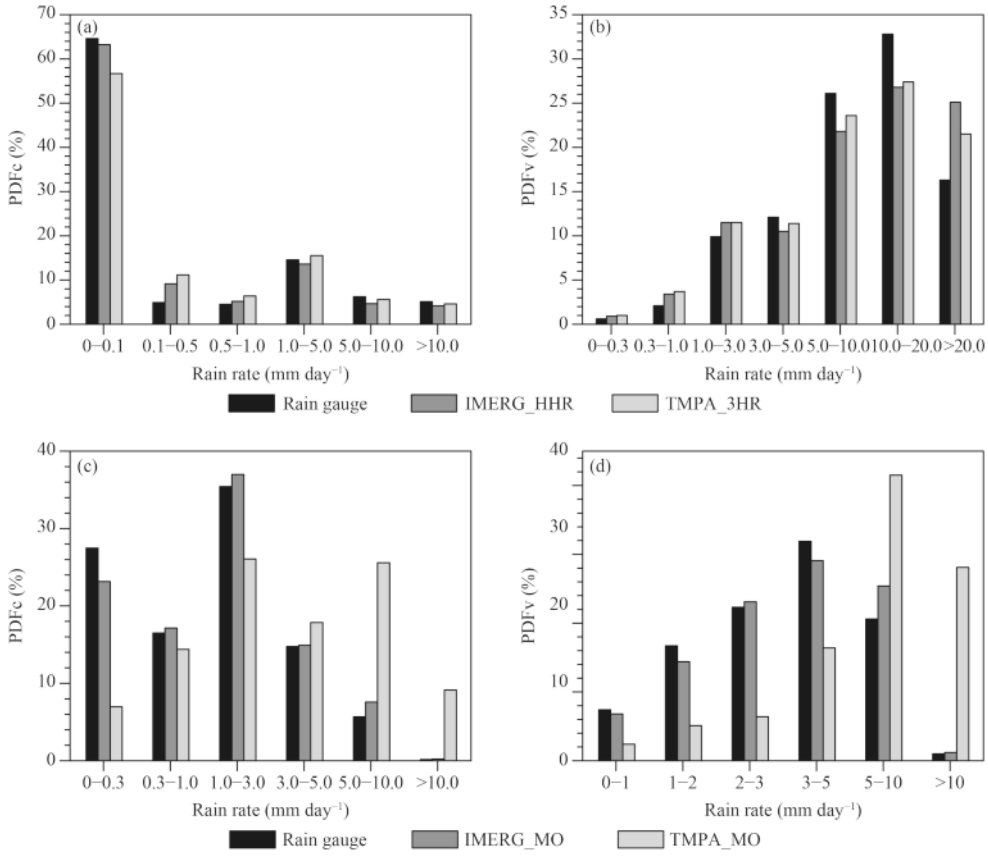

Fig. 6. PDFc and PDFv of (a, b) daily and (c, d) monthly precipitation with different rain rates, as derived from rain gauges, IMERG_HHR and TMPA_3HR, and IMERG_MO and TMPA_MO.

(3–20 mm day^{-1}), as indicated in Fig. 6b. Nevertheless, when the rain rate is more than 20 mm day^{-1}, both satellite products can detect larger rainfall volumes over the TP, but TMPA_3HR performs better than IMERG_HHR, which calls for special attention from the algorithm developers. On the monthly timescale, IMERG_MO improves the detection ability in terms of both the occurrence frequency (Fig. 6c) and the rainfall volume (Fig. 6d), across all rain-rate categories.

In order to assess the detection capability for different rainfall intensities, and explain the obvious discrepancies for TMPA_MO in Figs. 6c and 6d, Fig. 7 shows the differences between the PDFc of rain gauges and that of the satellite precipitation products on the daily and monthly timescales under different rainfall ranges. The dots in green or blue represent underestimation by the satellite products, and dots in yellow or red represent overestimation. On the daily timescale, the performances of IMERG and TMPA in detecting light, moderate and heavy precipitation events are remarkably similar, regardless of the precipitation intensity, as determined by comparing the plots in the first row (Figs. 7a–c) and the second row (Figs. 7d–f). On the monthly scale, the detection ability of IMERG outperforms that of TMPA because of much smaller discrepancies for IMERG. Both satellite precipitation products tend to underestimate the occurrence of light rainfall events (less than 5 mm day^{-1}) over most of the TP (85.7% stations for IMERG_MO, 92.4% stations for TMPA_MO). However, TMPA_MO shows more obvious underestimations, which are marked

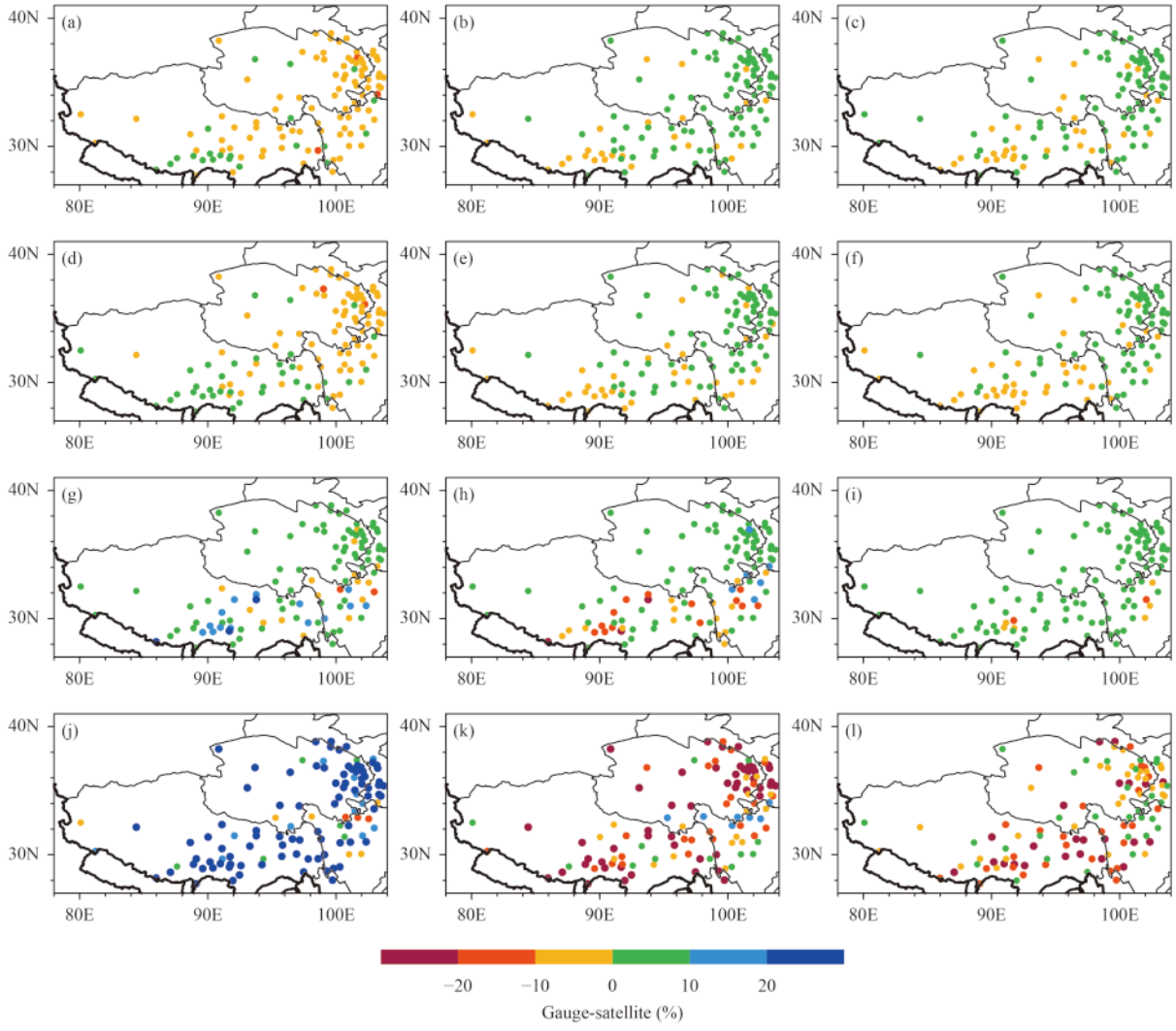

Fig. 7. Differences between the PDFc of rain gauges and those of (a–c) IMERG_HHR, (d–f) TMPA_3HR, (g–i) IMERG_MO, and (j–l) TMPA_MO, under the different rainfall ranges of (a, d, g, j) 0–5 mm day^{-1}, (b, e, h, k) 5–9 mm day^{-1}, and (c, f, i, l) > 9 mm day^{-1}, at stations over the TP. The differences are calculated as the former (PDFc of the rain gauges) minus the latter. The dots in green or blue represent underestimations by the satellite products, while the dots in yellow or red represent overestimations.

by dark-blue dots in Fig. 7j, while there are only nine (7.6%) stations where light precipitation events are overestimated by TMPA_MO. Although IMERG_MO overestimates the occurrence probability of 5–9 mm day^{-1} rainfall at only 26.1% stations over the TP, as shown in Fig. 7h, overestimations of these stations are generally greater than underestimations presented by the other 73.9% stations because of the overestimation presented by IMERG_MO for 5–10 mm day^{-1} rainfall in Fig. 6c. There are slight discrepancies (less than 10%) in the PDFc between IMERG_MO and the gauge measurements for heavy rainfall events larger than 9 mm day^{-1} (Fig. 7i), which demonstrates the adequate capability of IMERG_MO in detecting heavy rainfall. Nevertheless, contrasting sharply with IMERG_MO, TMPA_MO greatly overestimates the occurrence of moderate and heavy rainfall events over most of the TP, as shown in Figs. 7i, l, in which 92.4% and 74.0% of stations over the TP present overestimations for 5–9 mm day^{-1} and > 9 mm day^{-1} rainfall, respectively. These overestimations are also demonstrated in Fig. 6c, and the overestimations of the PDFv in Fig. 6d come from the excessive detection. By combining Figs. 7 and 6, we can better understand the seemingly abnormal overestimations of TMPA_MO for rainfall larger than 5 mm day^{-1}, and the superiority of IMERG_MO over the TP.

Figure 8 is a scatterplot of the daily and monthly satellite precipitation products over the TP. Both the IMERG_HHR and TMPA_3HR rainfall products show a general underestimation on the daily scale, as depicted in Figs. 8a, b. In general, the higher the daily rain rate, the more obvious the underestimation. As shown in Fig. 8c, IMERG_MO fits well with the rain-gauge data. TMPA_MO shows poor performance with remarkable overestimations (Fig. 8d). Thus, we can conclude that the IMERG products are superior to the TMPA products on the daily and monthly timescales. Scatterplots for the daily and monthly satellite products during the warm sea-

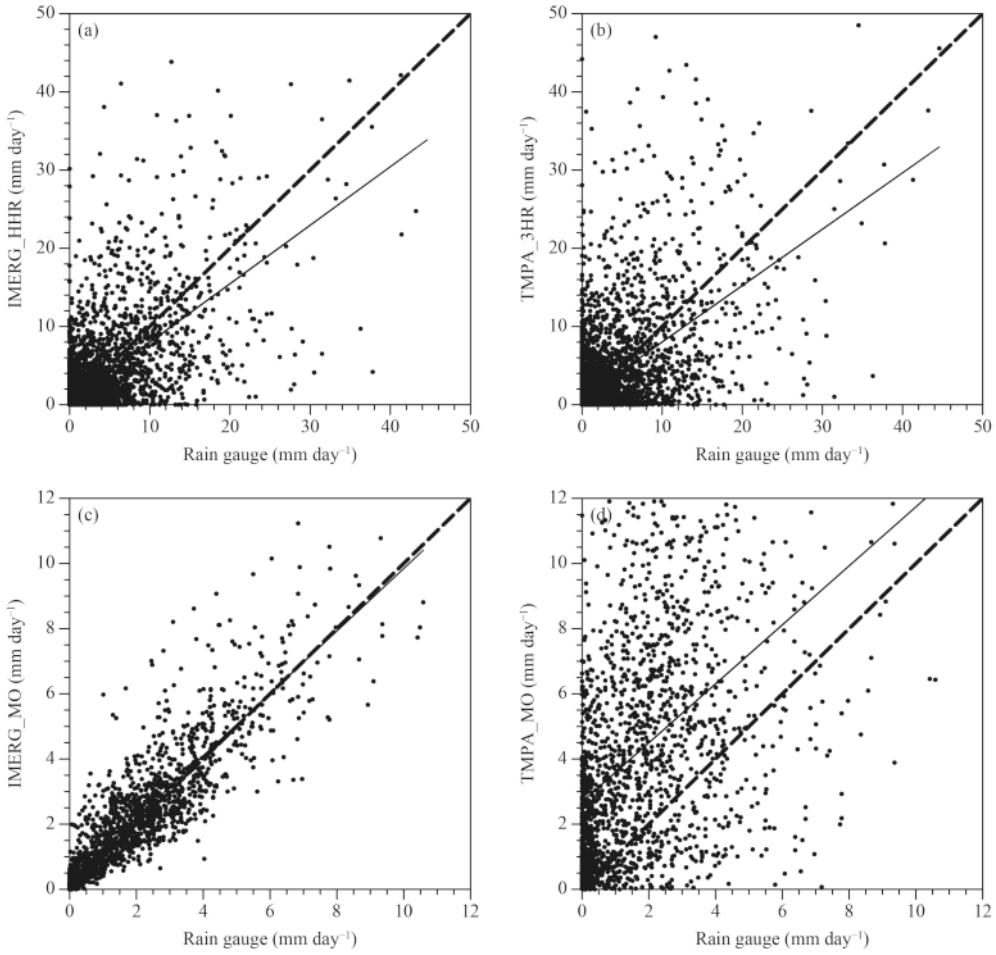

Fig. 8. Scatterplots of precipitation between the IMERG products, TMPA products, and rain-gauge data on the (a, b) daily and (c, d) monthly timescales during the whole study period. The diagonal reference line is indicated by a dash line, and the line of best (determined via the least-squares method) of all months is indicated by a solid line.

son, from May to October, were also plotted (omitted), from which it was found that the aforementioned characteristics are more obvious during the summer season.

The level of concordance between satellite observations and rain-gauge measurements on the daily scale is explored in Fig. 9. The CC and RMSE between IMERG_HHR and the rain-gauge data are shown in Figs. 9a, b, respectively, while the CC and RMSE between TMPA_3HR and the rain-gauge data are shown in Figs. 9c, d. The IMERG data reveal a high degree of correlation for up to 81.42% of rain-gauge stations over the TP, based on the fact that the CC of IMERG is higher than that of TMPA among those stations. In terms of the RMSE, which is usually used to describe the error and bias of satellite estimates compared with gauge observations, the IMERG data reveal a lower deviation, as evidenced by the RMSE of IMERG being smaller for 63.72% of rain-gauge stations, and both satellite products showing similar RMSE patterns geographically over the TP, decreasing gradually from the southeast to northwest, as shown in Figs. 9b, d. Spatially, IMERG_HHR shows lower deviation and better correlation with most rain gauges than TMPA_3HR over the whole TP.

The variations in the evaluation metrics (BIAS, HKS, POD, and FAR) with increasing elevation are investigated in Fig. 10. In general, these evaluation metrics do not exhibit strong correlation with the varying topographic elevation. However, IMERG_HHR again demonstrates better capability in correctly capturing daily rainfall events compared with TMPA_3HR, with higher HKS and POD and lower FAR. Besides, IMERG_HHR ameliorates the overestimation obviously, supported by the bias being closer to 1.

4. Summary

This study evaluates the GPM IMERG rainfall products and compares their performances with the TRMM TMPA rainfall products on multiple timescales over the TP. High-quality hourly observations from 113 national-level rain-gauge stations are used as reference. The main conclusions are as follows:

(1) The evaluations of GPM IMERG_HHR on the hourly timescale using ground-based rain-gauge measurements as a reference show the ability of IMERG_HHR to describe the hourly rainfall intensity, and thus to characterize the diurnal variation of rainfall over the TP with very high temporal resolution. However, discrepancies in

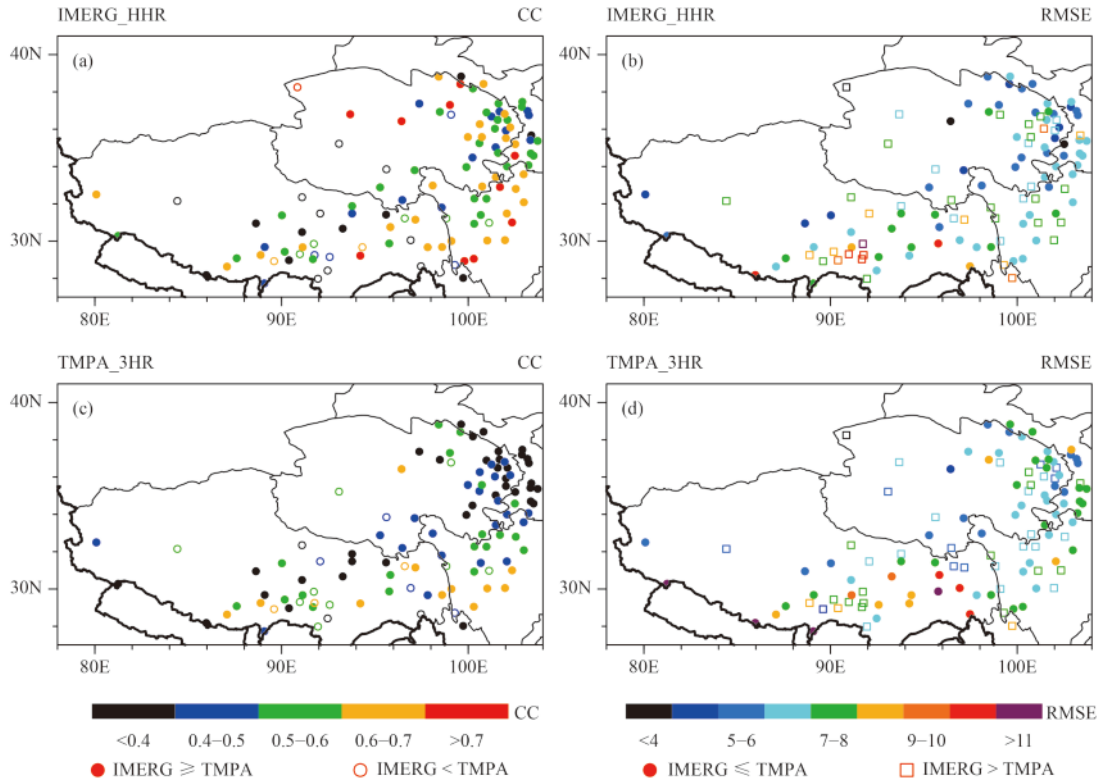

Fig. 9. Maps of the (a, c) CC and (b, d) RMSE between IMERG_HHR, TMPA_3HR, and rain-gauge data on the daily timescale. The CC and RMSE values are represented by the color bars under their respective panels. The units for the RMSE are mm day^{-1}. The dots are indices, based on the CC or RMSE, of IMERG_HHR performing better than TMPA_3HR.

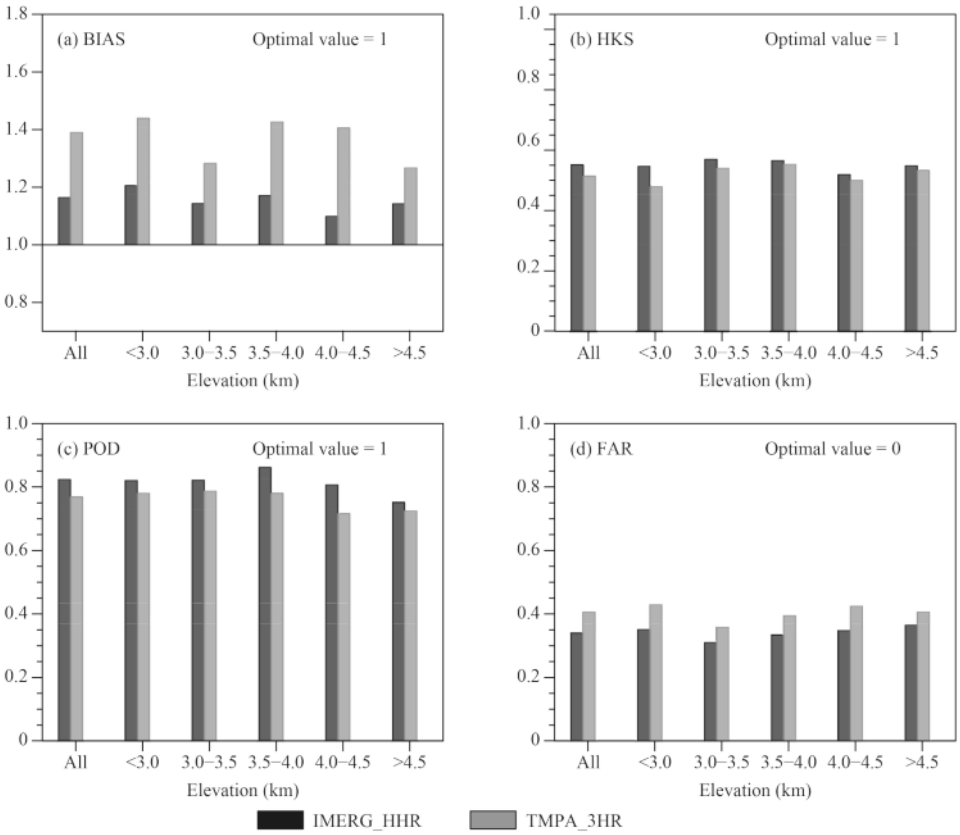

Fig. 10. The (a) bias, (b) HKS, (c) POD, and (d) FAR from the IMERG_HHR and TMPA_3HR products on the daily timescale over different elevation ranges.

the timing of the greatest rainfall intensity between IMERG_HHR and rain gauges exist. Besides, IMERG_HHR tends to underestimate the occurrence frequency of the rainfall peak from early afternoon to evening, and overestimate the frequency of the peak from nighttime to early morning. Geographically, IMERG_HHR overestimates the maximum rainfall intensity over the whole of the TP. The capability of IMERG_HHR in reproducing the diurnal variation could be acceptable, but caution should be exercised by algorithm developers and users.

(2) On the hourly scale, IMERG_HHR performs differently above and below the elevation threshold of 3500 m. The normalized pattern statistics at elevations below 3500 m are better than those above 3500 m, as indicated by the larger CC, lower relative bias, and the ratio of the standard deviation being closer to 1 for the former.

(3) The GPM IMERG products generally perform better than the TRMM TMPA products on the daily and monthly timescales. IMERG_HHR captures the occurrence frequency and total volume of light precipitation events better than TMPA_3HR, although IMERG_HHR overestimates the PDFv of heavy rainfall (more than 20 mm day^{-1}) more obviously than TMPA_3HR. IMERG_MO outperforms TMPA_MO under different rainfall ranges in terms of PDFc and PDFv, and IMERG_MO shows better detection capability for all rainfall events over the TP. IMERG is superior to TMPA, with higher correlation, lower deviation and a smaller overestimation across the TP. In addition, the capability of IMERG_HHR in correctly capturing daily rainfall events, in comparison with TMPA_3HR, is better over different elevation ranges, with higher HKS and POD and lower FAR.

Although the 21-month study period used here might be deemed insufficient to draw general climatological conclusions about the trends in the spatiotemporal variation of precipitation from satellite observations, our research nevertheless serves as a preliminary investigation of the precipitation over the TP using IMERG over a reasonably long period. Besides, the reference data from the hourly updated ground-based rain gauges validate the general improvement of IMERG over TMPA. Furthermore, these evaluations on multiple timescales, albeit within the specific scenario of the TP, have the potential to provide some valuable feedback to algorithm developers. Further studies that explore the capability of IMERG in detecting and depicting individual extreme precipitation over complex mountainous regions would

be a useful next step in this line of research.

Acknowledgments. The IMERG Final Run data were provided by the NASA/Goddard Space Flight Center's Mesoscale Atmospheric Processes Laboratory and PPS, which develop and compute the IMERG as a contribution to GPM, and are archived at the NASA GES DISC (https://pmm.nasa.gov/data-access/downloads/gpm). The TRMM 3B42V7 and 3B43 data were provided by the NASA/Goddard Space Flight and obtained freely online at https://pmm.nasa.gov/data-access/downloads/trmm. We acknowledge the editor and anonymous reviewers for their insightful and constructive comments, which helped improve the original manuscript substantially.

REFERENCES

Andermann, C., L. Longuevergne, S. Bonnet, et al., 2012: Impact of transient groundwater storage on the discharge of Himalayan rivers. *Nature Geosci.*, **5**, 127–132, doi: 10.1038/ngeo1356.

Bai, A. J., C. H. Liu, and X. D. Liu, 2008: Diurnal variation of summer rainfall over the Tibetan Plateau and its neighboring regions revealed by TRMM multi-satellite precipitation analysis. *Chinese J. Geophys.*, **51**, 518–528, doi: 10.1002/cjg2.1242.

Chen, F. R., and X. Li, 2016: Evaluation of IMERG and TRMM 3B43 monthly precipitation products over mainland China. *Remote Sens.*, **8**, 472, doi: 10.3390/rs8060472.

Cimini, D., F. Romano, E. Ricciardelli, et al., 2013: Validation of satellite OPEMW precipitation product with ground-based weather radar and rain gauge networks. *Atmos. Meas. Tech.*, **6**, 3181–3196, doi: 10.5194/amt-6-3181-2013.

Dai, A., F. Giorgi, and K. E. Trenberth, 1999: Observed and model-simulated diurnal cycles of precipitation over the contiguous United States. *J. Geophys. Res.*, **104**, 6377–6402, doi: 10.1029/98JD02720.

Ebert, E. E., J. E. Janowiak, and C. Kidd, 2007: Comparison of near-real-time precipitation estimates from satellite observations and numerical models. *Bull. Amer. Meteor. Soc.*, **88**, 47–64, doi: 10.1175/BAMS-88-1-47.

Fujinami, H., S. Nomura, and T. Yasunari, 2005: Characteristics of diurnal variations in convection and precipitation over the southern Tibetan Plateau during summer. *Sola*, **1**, 49–52, doi: 10.2151/sola.2005-014.

Gao, Y. C., and M. F. Liu, 2013: Evaluation of high-resolution satellite precipitation products using rain gauge observations over the Tibetan Plateau. *Hydrol. Earth Syst. Sci.*, **17**, 837–849, doi: 10.5194/hess-17-837-2013.

Guo, J. P., P. M. Zhai, L. Wu, et al., 2014: Diurnal variation and the influential factors of precipitation from surface and satellite measurements in Tibet. *Int. J. Climatol.*, **34**, 2940–2956, doi: 10.1002/joc.3886.

Guo, H., S. Chen, A. M. Bao, et al., 2016: Early assessment of integrated multi-satellite retrievals for global precipitation measurement over China. *Atmos. Res.*, **176–177**, 121–133, doi: 10.1016/j.atmosres.2016.02.020.

Hong, Y., K. L. Hsu, S. Sorooshian, et al., 2004: Precipitation estimation from remotely sensed imagery using an artificial neural network cloud classification system. *J. Appl. Meteor.*, **43**, 1834–1853, doi: 10.1175/JAM2173.1.

Hou, A. Y., R. K. Kakar, S. P. Neeck, et al., 2014: The global precipitation measurement mission. *Bull. Amer. Meteor. Soc.*, **95**, 701–722, doi: 10.1175/BAMS-D-13-00164.1.

Hsu, K. L., X. G. Gao, S. Sorooshian, et al., 1997: Precipitation estimation from remotely sensed information using artifical neural networks. *J. Appl. Meteor.*, **36**, 1176–1190, doi: 10.1175/1520-0450(1997)036<1176:PEFRSI>2.0.CO;2.

Huffman, G. J., D. T. Bolvin, E. J. Nelkin, et al., 2007: The TRMM Multisatellite Precipitation Analysis (TMPA): Guasi-global, multiyear, combined-sensor precipitation estimates at fine scales. *J. Hydrometeorol.*, **8**, 38–55, doi: 10.1175/JHM560.1.

Joyce, R. J., J. E. Janowiak, P. A. Arkin, et al., 2004: CMORPH: A method that produces global precipitation estimates from passive microwave and infrared data at high spatial and temporal resolution. *J. Hydrometeorol.*, **5**, 487–503, doi: 10.1175/1525-7541(2004)005<0487:CAMTPG>2.0.CO;2.

Kidd, C., and V. Levizzani, 2011: Status of satellite precipitation retrievals. *Hydrol. Earth Syst. Sci.*, **15**, 1109–1116, doi: 10.5194/hess-15-1109-2011.

Kidd, C., P. Bauer, J. Turk, et al., 2012: Intercomparison of high-resolution precipitation products over northwest Europe. *J. Hydrometeorol.*, **13**, 67–83, doi: 10.1175/JHM-D-11-042.1.

Kirstetter, P. E., Y. Hong, J. J. Gourley, et al., 2013: Comparison of TRMM 2A25 products, version 6 and version 7, with NOAA/NSSL ground radar-based national mosaic QPE. *J. Hydrometeorol.*, **14**, 661–669, doi: 10.1175/JHM-D-12-030.1.

Liu, L. P., J. M. Feng, R. Z. Chu, et al., 2002: The diurnal variation of precipitation in monsoon season in the Tibetan Plateau. *Adv. Atmos. Sci.*, **19**, 365–378, doi: 10.1007/s00376-002-0028-6.

Liu, Z., 2016: Comparison of Integrated Multisatellite Retrievals for GPM (IMERG) and TRMM Multisatellite Precipitation Analysis (TMPA) monthly precipitation products: Initial results. *J. Hydrometeorol.*, **17**, 777–790, doi: 10.1175/JHM-D-15-0068.1.

Ma, Y. Z., G. Q. Tang, D. Long, et al., 2016: Similarity and error intercomparison of the GPM and its predecessor-TRMM Multisatellite Precipitation Analysis using the best available hourly gauge network over the Tibetan Plateau. *Remote Sens.*, **8**, 569, doi: 10.3390/rs8070569.

Oliveira, R., V. Maggioni, D. Vila, et al., 2016: Characteristics and diurnal cycle of GPM rainfall estimates over the central Amazon region. *Remote Sens.*, **8**, 544, doi: 10.3390/rs8070544.

Prakash, S., A. K. Mitra, A. AghaKouchak, et al., 2016: A preliminary assessment of GPM-based multi-satellite precipitation estimates over a monsoon dominated region. *J. Hydrol.*, **556**, 865–876, doi: 10.1016/j.jhydrol.2016.01.029.

Prat, O. P., and B. R. Nelson, 2013: Precipitation contribution of tropical cyclones in the southeastern United States from 1998 to 2009 using TRMM satellite data. *J. Climate*, **26**, 1047–1062, doi: 10.1175/JCLI-D-11-00736.1.

Sapiano, M. R. P., and P. A. Arkin, 2009: An intercomparison and validation of high-resolution satellite precipitation estimates with 3-hourly gauge data. *J. Hydrometeorol.*, **10**, 149–166, doi: 10.1175/2008JHM1052.1.

Shen, Y., A. Y. Xiong, Y. Wang, et al., 2010: Performance of high-resolution satellite precipitation products over China. *J. Geophys. Res.*, **115**, D02114, doi: 10.1029/2009JD012097.

Shen, Y., P. Zhao, Y. Pan, et al., 2014: A high spatiotemporal gauge-satellite merged precipitation analysis over China. *J. Geophys. Res.*, **119**, 3063–3075, doi: 10.1002/2013JD020686.

Shige, S., S. Kida, H. Ashiwake, et al., 2013: Improvement of TMI rain retrievals in mountainous areas. *J. Appl. Meteor. Climatol.*, **52**, 242–254, doi: 10.1175/JAMC-D-12-074.1.

Simpson, J., R. F. Adler, and G. R. North, 1988: A proposed tropical rainfall measuring mission (TRMM) satellite. *Bull. Amer. Meteor. Soc.*, **69**, 278–295, doi: 10.1175/1520-0477(1988)069<0278:APTRMM>2.0.CO;2.

Singh, P., and K. Nakamura, 2009: Diurnal variation in summer precipitation over the central Tibetan Plateau. *J. Geophys. Res.*, **114**, D20107, doi: 10.1029/2009JD011788.

Sorooshian, S., K. L. Hsu, X. G. Gao, et al., 2000: Evaluation of PERSIANN system satellite-based estimates of tropical rainfall. *Bull. Amer. Meteor. Soc.*, **81**, 2035–2046, doi: 10.1175/1520-0477(2000)081<2035:EOPSSE>2.3.CO;2.

Tang, G. Q., Y. Z. Ma, D. Long, et al., 2016: Evaluation of GPM Day-1 IMERG and TMPA version-7 legacy products over mainland China at multiple spatiotemporal scales. *J. Hydrol.*, **533**, 152–167, doi: 10.1016/j.jhydrol.2015.12.008.

Taylor, K. E., 2001: Summarizing multiple aspects of model performance in a single diagram. *J. Geophys. Res.*, **106**, 7183–7192, doi: 10.1029/2000JD900719.

Tong, K., F. G. Su, D. Q. Yang, et al., 2014: Evaluation of satellite precipitation retrievals and their potential utilities in hydrologic modeling over the Tibetan Plateau. *J. Hydrol.*, **519**, 423–437, doi: 10.1016/j.jhydrol.2014.07.044.

Wen, Y. X., A. Behrangi, B. Lambrigtsen, et al., 2016: Evaluation and uncertainty estimation of the latest radar and satellite snowfall products using SNOTEL measurements over mountainous regions in western United States. *Remote Sens.*, **8**, 904, doi: 10.3390/rs8110904.

Wolff, D. B., and B. Fisher, 2009: Assessing the relative performance of microwave-based satellite rain-rate retrievals using TRMM ground validation data. *J. Appl. Meteor. Climatol.*, **48**, 1069–1099, doi: 10.1175/2008JAMC2127.1.

Xu, R., F. Q. Tian, L. Yang, et al., 2017: Ground validation of GPM IMERG and TRMM 3B42V7 rainfall products over southern Tibetan Plateau based on a high-density rain gauge network. *J. Geophys. Res.*, **122**, 910–924, doi: 10.1002/2016JD025418.

Yong, B., Y. Hong, L. L. Ren, et al., 2012: Assessment of evolving TRMM-based multisatellite real-time precipitation estimation methods and their impacts on hydrologic prediction in a high latitude basin. *J. Geophys. Res.*, **117**, D09108, doi: 10.1029/2011JD017069.

Tech & Copy Editor: Yi ZHANG